Tectonophysics 869 (2023) 230148

Contents lists available at ScienceDirect

Tectonophysics

journal homepage: www.elsevier.com/locate/tecto

Paleomagnetic study of Late-Carboniferous-Permian rocks from the Cadí Basin (Eastern Pyrenees): Tectonic implications

Ana Simón-Muzás [a,*], Antonio M. Casas-Sainz [a], Ruth Soto [b], Emilio L. Pueyo [b], Elisabet Beamud [c], Belén Oliva-Urcia [a]

[a] Departamento de Ciencias de la Tierra, Geotransfer-IUCA, Universidad de Zaragoza, 50009 Zaragoza, Spain
[b] IGME, Instituto Geológico y Minero de España, Unidad de Zaragoza, 50006 Zaragoza, Spain
[c] Paleomagnetic Laboratory CCiTUB - Geosciences Barcelona (Geo3Bcn), CSIC, 08028 Barcelona, Spain

ARTICLE INFO

Keywords:
Paleomagnetism
Volcanic
Red beds
Late Carboniferous
Permian
Pyrenees

ABSTRACT

We have carried out a detailed paleomagnetic study of volcanic rocks (18 sites) and red beds (10 sites) from the Late-Carboniferous-Permian series of the Cadí Basin (Eastern Pyrenees). The study provides reliable Late Carboniferous-Permian paleomagnetic directions, in an area where paleomagnetic studies are scarce. The main characteristic component in both rock types shows a SSE direction with a shallow inclination and a dominant reverse polarity. The magnetic carriers, both in the volcanic rocks and the red beds, are magnetite and hematite. The main component is interpreted as a primary magnetization of Permian age in the red beds; in the Late Carboniferous volcanic rocks, the main component likely represents primary magnetization or early remagnetization. These results are consistent with the poles for the Iberian plate during the Permian and indicate an absence of regional vertical axis rotations for the Orri nappe, in whose hanging wall the Cadí Basin was transported southwards during the Pyrenean orogeny.

1. Introduction

In spite of the difficulties in interpreting paleomagnetic directions in fold-and-thrust belts (Pueyo et al., 2016a), primary magnetizations can be used to unravel plate motions (Gong et al., 2008; Vissers and Meijer, 2012) and thrust-related kinematics (McCaig and McClelland, 1992; Oliva-Urcia and Pueyo, 2007 and 2019). In Iberia, the occurrence of widespread remagnetizations can preclude the use of paleomagnetic directions with such objectives. Nevertheless, secondary magnetizations may help to infer the deformational history of thrust belts and to obtain valuable kinematic information (e.g., Villalaín et al., 2016; Soto et al., 2008, 2011; Torres-López et al., 2018). In the Pyrenees there are three remagnetization events, dated as Permian (Pastor-Galán et al., 2021), Early Cretaceous (Larrasoaña et al., 2003; Garcés et al., 2016) and Eocene-Oligocene (Oliva-Urcia and Pueyo, 2007; Oliva-Urcia et al., 2008, 2012; Izquierdo-Lavall et al., 2015; Izquierdo-Llavall et al., 2018). These remagnetization events erased the primary magnetization of the rocks located within internal units of the orogen. Nevertheless, the occurrence of secondary magnetizations or the co-existence of primary and secondary magnetizations have not precluded the extensive use of paleomagnetism for the determination of the kinematics of thrusts. The differences in displacement within a thrust sheet can be detected by means of vertical axis rotations inferred from paleomagnetic methods (Sussman et al., 2012; Pueyo et al., 2016a). In this sense, paleomagnetism has become an important complementary tool for defining basin-scale or crustal-scale cross-sections.

In this work, we focus on the Late Carboniferous-Permian Cadí Basin, which is a sector of the Pyrenees for which paleomagnetic data are relatively scarce (Pueyo et al., 2016b and references therein). The study area is located at the southern margin of the Axial Zone in the Eastern Pyrenees (Fig. 1 A and B). The typical stratigraphic sequence in this area consists of volcanic, volcaniclastic, and continental sedimentary rocks that were deposited in small, variably-spaced intra-mountain basins. These basins have undergone significant transport in the hanging wall of one of the most important basement thrust sheets that define the Pyrenean orogen (e.g. Gisbert, 1981).

Previous work in the area, by Van Dongen (1967), recognized an Early Permian paleomagnetic component (Dec 169.5° and Inc. −3°) in Carboniferous volcanic rocks. This vector was used to define an Early Permian pole (48.5° N, 163° W) for the Iberian plate. Based on these

* Corresponding author.
E-mail address: anasimon@unizar.es (A. Simón-Muzás).

https://doi.org/10.1016/j.tecto.2023.230148
Received 26 January 2023; Received in revised form 17 November 2023; Accepted 18 November 2023
Available online 25 November 2023

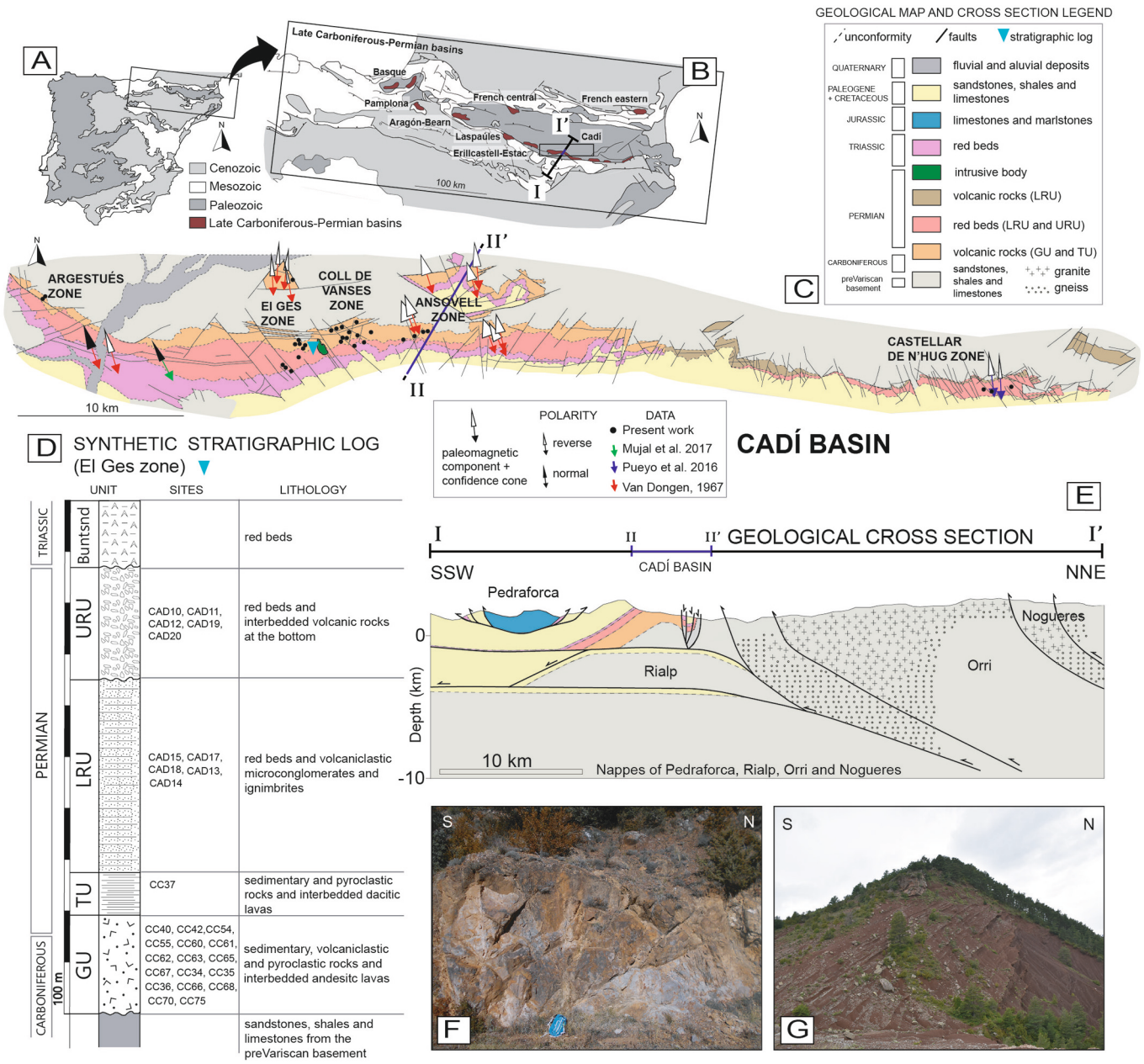

Fig. 1. A) Geological map of the Iberian Peninsula; B) Geological map of the Pyrenees with the Carboniferous-Permian basins highlighted in maroon (modified from Izquierdo-Llavall et al., 2013); C) Simplified geological map of the Late-Carboniferous-Permian Cadí Basin and the studied areas: Argestués, Coll de Vanses, Ansovell and Castellar de n'Hug (modified from Gisbert, 1981); D) Synthetic stratigraphic log; E) Geological cross sections: I-I') General view (simplified from Soto et al., 2022) and II-II') Location of the Cadí Basin; views of the studied outcrops: F) Field photograph of an exposure of volcanic and volcaniclastic rocks (site CC60), G) Photograph showing the red beds (site CAD12). (For interpretation of the references to colour in this figure legend, the reader is referred to the web version of this article.)

results, Van Dongen (1967) inferred that the Iberian Peninsula was subjected to a post-Permian counter-clockwise rotation of 30°. Pueyo et al. (2016b) recognized a primary magnetization component in the red beds from the easternmost part of the Cadí Basin, in the Castellar de n'Hug area (Fig. 1 C). This component shows a direction similar to the one obtained by Van Dongen (1967) for the volcanic rocks. Pueyo et al. (2016b) also isolated an intermediate-temperature reverse paleomagnetic component, in the sedimentary rocks of this unit. A magnetostratigraphic study of the Permian red beds was performed by Mujal et al. (2017) in the western part of the Cadí Basin. However, a generalized remagnetization precluded the application of magnetostratigraphic analysis. This scarcity of paleomagnetic data, and the uncertainty in the previous results, have motivated the present study, that aims: 1) to characterize the Permian remagnetization event recognized in other zones of the Pyrenees (Pastor-Galán et al., 2021) and 2) to reconstruct the kinematics of the Alpine Orri thrust sheet (that has transported the Cadí Basin in its hanging wall). We finally compare our results with neighboring structures, where the existence of vertical axis rotations has been demonstrated (Izquierdo-Llavall et al., 2013). The possibility of comparing the results obtained in volcanic and volcaniclastic deposits on one side and red beds on the other, can also provide interesting information on the origin of the paleomagnetic components.

2. Geological setting

The study area is located in the Cadí Basin, one of the Late

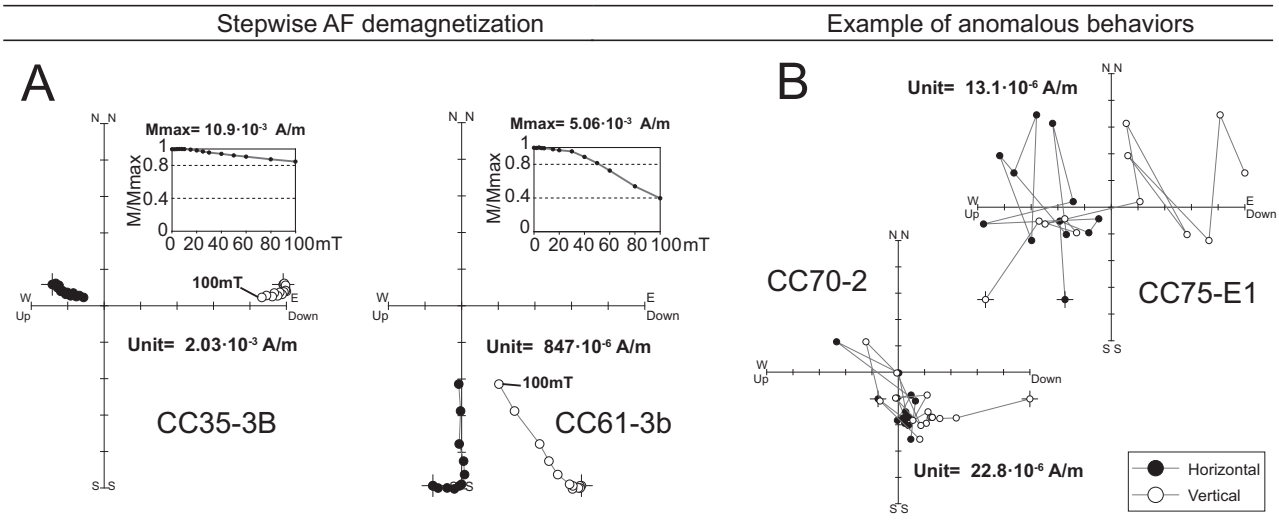

Fig. 2. A) stepwise AF demagnetization from 0 to 100mT in two pilot specimens from volcanic and volcaniclastic rocks. B) Examples of anomalous behavior in sites CC70 and CC75. In white colour, vertical projection and in black colour, horizontal projection, N upward and E to the right. Additionally, normalized intensity of the NRM (M/Mmax) versus temperature diagrams are shown.

Carboniferous-Permian basins located at the southern border of the Pyrenees (Fig. 1 A and B). The Cadí Basin (Fig.1 C and E) is a 30 km-long intra-mountain basin oriented in an approximately WNW-ESE direction. It has been interpreted as an asymmetric graben, which is limited by extensional faults to the north and south (Saura and Teixell, 2006). At present, its sedimentary infill forms a south-dipping monocline, which belongs to the southern limb of a basin-scale anticline associated with the Alpine, basement-involved, Orri thrust (Muñoz et al., 1986; Saura and Teixell, 2006). The structure of the Cadí Basin is the result of a positive tectonic inversion; it underwent two main rift-postrift Late Paleozoic-Mesozoic cycles that affected the Variscan basement (e.g. Barnolas and Pujalte, 2004). Subsequently, during the Pyrenean compression, the basin was subjected to shortening. The latter stage can be bracketed between the Early Eocene and the Late Oligocene (Vergés et al., 2002). During the Alpine orogeny, the Cadí Basin was incorporated into the south-verging Orri thrust sheet (Muñoz et al., 1986; Muñoz, 1992; Saura and Teixell, 2006), that contains rocks of Paleozoic and Triassic age (e.g. Muñoz, 1992).

In the Cadí Basin, the following units can be distinguished (Fig. 1 D), according to the stratigraphic subdivision proposed by Gisbert (1981): Grey Unit, Transition Unit, Lower Red Unit and Upper Red Unit. The Grey Unit (GU) lies unconformably on the Variscan basement (Ordovician to Devonian rocks, Casas et al., 2012). It is composed of breccias, sandstones, conglomerates, grey siltstones and layers of coal. This sedimentary sequence passes laterally to volcaniclastic and pyroclastic rocks with interbedded andesitic lava flows (Fig. 1 F). The Transition unit (TU) is characterized by conglomerates, sandstones and siltstones. In this unit, sedimentary rocks show a lateral transition to pyroclastic rocks with interbedded dacitic lavas. The Lower Red Unit (LRU) is mainly composed of siltstones, sandstones, acidic tuffs and red volcaniclastic microconglomerates. In the Cadí Basin, these lithologies interfinger with pyroclastic rocks that contain ignimbrites and interbedded banded rhyolites. Finally, the Upper Red Unit (URU) contains red conglomerates, sandstones, and siltstones (Fig. 1 G) with carbonate nodules, and lacustrine deposits. These rocks are arranged in two sequences, with interbedded volcanic bodies at the bottom. Mafic minerals and plagioclases in the volcanic series are replaced by opaque minerals, chlorite, ferromagnesian silicates, carbonates and sericite (Gisbert, 1981; Bixel, 1984). Radiometric dating of extrusive rocks of the GU in the Cadí Basin yielded Late Carboniferous ages, including 304.0 ± 1.5 Ma (andesite) and 300.4 ± 1.4 Ma (ignimbrite) (Pereira et al., 2014).

3. Methodology

The 28 sites are distributed along N-S and NW-SE cross-sections (El Ges, Coll de Vanses and Ansovell transects) as well as in specific zones of the basin margins (Argestués and Castellar de n'Hug outcrops). A total of 18 sampling sites (158 specimens) were taken in Late Carboniferous-Permian volcanic and volcaniclastic rocks (GU and TU), and 10 sites (77 specimens) in Permian red beds (sandstones and siltstones, LRU and URU). Sites were grouped according to their lithology: Carboniferous-Permian volcanic-volcaniclastic materials on one side and Permian terrigenous red beds on the other. Sampling was aimed to obtain data from different age intervals and to compare results obtained in rocks bearing different magnetic properties.

We avoided sampling the northern area of the Cadi Basin where the main structures are smaller in size and Carboniferous-Permian rocks are found in isolated grabens. In addition, data for these zones have been made available from paleomagnetic data obtained by other authors (Fig. 1 C). A proper fold test could not be carried out because the stratigraphic sequence is arranged as a south-dipping, gentle monocline. The conglomerate tests performed for a lava breccia were not conclusive, and consequently those results were not further considered (sites T08, T100, T102).

The samples were taken directly in the field as standard paleomagnetic cylindrical cores with a gasoline-powered drill machine (26 sites) or as oriented blocks taken with extraction tools (two sites: CAD18 and CAD19). In the laboratory, the oriented cores and blocks were cut to standard oriented specimens using a radial saw (non-magnetic steel). The average number of cores per site was nine, with a minimum of six at site CC35 and a maximum of 10 in several volcanic-rocks sites.

Paleomagnetic analyses were conducted in two laboratories. Two pilot sites (CC35 and CC61) were demagnetized with a 2G cryogenic magnetometer with an alternating field (AF) demagnetizer in the Paleomagnetism laboratory at the University of Burgos (Spain). Two specimens from the two pilot sites were firstly demagnetized by an alternating field from 0 to 100 mT; however, magnetization was not fully removed after 100 mT (Fig. 2 A). For this reason, we discarded AF demagnetization (see supplementary material), and, instead, we applied thermal demagnetization (Th) to the remaining samples from room temperature up to 670 °C (16 steps) with a TD48-DC thermal demagnetizer. The Th demagnetization of the other specimens was carried out in the Paleomagnetic Laboratory CCiTUB-Geosciences Barcelona (CSIC) (Spain) using the TD48EU (ASC Scientific) and TSD-1 (Schondstedt)

Table 1
Paleomagnetic data at site level of the high temperature component in volcanic and volcaniclastic rocks (Ch). Sampled section and name of the site, coordinates (longitude and latitude), N: number of samples used to calculate the mean from the total number, Nt: number of total standard samples, Unit: stratigraphic unit, Grey Unit (GU), Transition Unit (TU); site-mean NRM value, Km: site-mean susceptibility value, Declination (Dec) and Inclination (Inc) before (BTC) and after (ATC) tectonic correction, α_{95} and k are the statistical parameters of a fisherian distribution (Fisher, 1953); Quality: good: $\alpha_{95} < 15$, intermediate: $\alpha_{95} = 15$ to 25, bad (out of threshold): $\alpha_{95} > 25$, D: declination error (calculated as D = arcsin (sin α_{95} /cos[I]), S0: bedding plane (dip direction and dip).

		ETR89 UTM zone31N EPSG: 25831		High temperature component (Ch)													
	Site	Longitude	Latitude	N	Nt	Unit	NRM(A/m) ($\cdot10^{-3}$)	Km($\cdot10^{-6}$)	Dec BTC	Inc BTC	α_{95}	Quality	D	k	Dec ATC	Inc ATC	S0 (D·D/Dip)
El Ges	CC34 *	1.501574	42.302963	8	8	GU	180	800	241	27.8	55.5	bad	56.2	1.95	227.6	−7.5	170/72
	CC35 *	1.501684	42.302798	–	6	GU	–	–	–	–	–	–	–	–	–	–	180/90
	CC36	1.501775	42.302627	9	9	GU	28.7	1053	233.9	33.1	64.9	bad	79.7	1.59	227.3	−23.0	180/80
	CC37	1.501771	42.302481	9	9	TU	7	575	133	35.9	53.5	bad	74.8	1.88	134.7	−33.6	180/75
	CC40	1.499777	42.302595	10	10	GU	9.24	310	150.8	34.1	7.5	good	7.5	42.97	152.7	−5.3	162/40
	CC42	1.582011	42.306753	9	9	GU	9.27	399	156	27	1.5	good	1.5	1175.2	162.3	−5.7	204/45
Ansovell	CC54+	1.585579	42.310182	10	10	GU	11.07	632	278.2	16.8	3.4	good	6.8	201.86	286	−60.1	270/78
	CC55	1.587445	42.311082	9	9	GU	90.08	386	156.3	22.4	2.2	good	2.6	531.26	152.5	−32.4	190/65
	CC60	1.535565	42.306902	9	9	GU	46	1045	149	38.6	4.1	good	4.1	157.9	156.2	−3.7	180/47
	CC61	1.531243	42.308103	7	7	GU	7.03	322	140.1	48.7	6.2	good	6.3	96.86	146.8	−9.4	160/60
				6	8				115.8	53.2	13.4	good	13.5	26.05	135.2	6.2	
	CC62	1.530810	42.308544	8★	8	GU	173.21	1044	139.9	46.2	36.4	bad	–	3.27	146.2	−6.8	160/55
Coll de Vanses	CC63	1.546480	42.311200	7	8	GU	60.2	546.2	151.9	17.1	3.1	good	3.1	319.14	156.1	−5.4	215/44
	CC65	1.529323	42.309946	8	8	GU	107	563	142.1	58.5	16.3	intermediate	16.3	12.44	161.3	−0.8	180/65
	CC66	1.529914	42.310323	10	10	GU	79.2	2025	141.6	63.9	6.4	good	7.1	65.22	180.5	26.1	205/54
	CC67	1.530015	42.310735	9	9	GU	58.4	549	133.4	66.9	11.6	good	12.8	20.55	149.9	24.6	177/42
	CC68	1.530407	42.311244	9	9	GU	5.92	302	126.7	52.2	5	good	5.0	107.70	152.3	3.2	183/63
Argestués	CC70 *	1.326368	42.323474	–	10	GU	–	–	–	–	–	–	–	–	–	–	207/38
	CC75 *	1.326915	42.323029	–	10	GU	–	–	–	–	–	–	–	–	–	–	200/45

*discarded sites: $\alpha_{95} > 25$ out of threshold or paleomagnetic component cannot be defined. + discarded sites: unknown paleomagnetic direction. ★ raw data

thermal demagnetizers, a JR-6 A spinner magnetometer (AGICO) and a superconducting rock magnetometer 755SRM (2G Enterprises). Magnetic susceptibility was measured after each demagnetization step with a KLY2 (Geofyzika Brno, now AGICO) in order to monitor the undesired creation of magnetic minerals during heating. No significant changes related to the neoformation of minerals were observed. The results of the progressive demagnetization were displayed on Zijderveld diagrams (Zijderveld, 1967) and the ChRM directions were analyzed using the software packages *Remasoft 3.0* (Chadima and Hrouda, 2006) and *VPD* (Ramón et al., 2017).

Lowrie's (1990) tests, (i.e. thermal demagnetization after acquisition of isothermal remanent magnetization, IRM, along three orthogonal axes) were conducted for five specimens: three in volcanic rocks and two in sedimentary red beds. In the volcanic rocks, samples CC35-3B, CC61-8 A and CC63–5 were magnetized using a pulse magnetizer. The imparted fields were 2, 0.4 and 0.147 T along the Z, Y, and X axes, respectively. They were measured in the 2G cryogenic magnetometer and were progressively demagnetized by means of a TD48 thermal demagnetizer at the Laboratory of Paleomagnetism, University of Burgos. For the sedimentary red beds, samples CAD12–8 and CAD15–10 were magnetized with imparted fields of 1.2, 0.3 and 0.1 T along the Z, Y, and X axes, respectively, by means of a IM10–30 impulse magnetizer (ASC Scientific) and were measured with a JR6A spinner magnetometer (AGICO) at the Paleomagnetic Laboratory CCiTUB-Geosciences Barcelona (CSIC).

We conducted temperature-dependent susceptibility experiments for 15 samples from different sites using a KLY-3S Kappabridge combined with a CS-3 furnace (temperature range 40°-700 °C) at the University of Zaragoza (Spain). These results were analyzed using the software SUSTE (AGICO Inc., Czech Republic). The selection criterion was based on previous AMS measurements (Simón-Muzás et al., 2022), by selecting the samples with representative K mean values for the two main lithologies: volcanic rocks and sedimentary red beds. The Cureval 8 software (Chadima and Hrouda, 2012) was used for the correction of the background signal (a measure of the empty CS3), the normalization of the susceptibility values to a specimen of a standard volume, and for the interpretation of the results.

The directional results for volcanic and volcaniclastic rocks and for Permian red beds are represented at the site level, the usual procedure for paleomagnetic data. For the quality control of the obtained paleomagnetic components, we used the criteria detailed below, defined according to the α_{95} involved in the Fisherian distribution at the site/locality level (Fisher, 1953). At the specimen level, we distinguished three categories taking into account the maximum angular deviation (MAD): 1 (MAD<10°); 2 (10° < MAD<25°); 3 (MAD>25°). At the site level, we defined three categories considering the α_{95} confidence cone: good ($\alpha_{95} < 15°$), intermediate ($15° < \alpha_{95} < 25°$); and bad ($\alpha_{95} > 25°$). Sites showing $\alpha_{95} > 25°$, were discarded from further interpretation (Table 1 and Table 2).

4. Results

4.1. NRM and magnetic mineralogy

The demagnetization of the natural remanent magnetization (NRM) of samples (Tables 1 and 2) at site level shows two slightly different behaviors depending on their lithology. The mean NRM intensities of the volcanic and volcaniclastic samples range between $5.92\cdot10^{-3}$ A/m and $180\cdot10^{-3}$ A/m showing a mean value of $58\cdot10^{-3}$ A/m. The magnetic susceptibility of these sites ranges between $302\cdot10^{-6}$ S·I. and $2025\cdot10^{-6}$ S.I. with a mean value of $703\cdot10^{-6}$ S.I. The Permian red beds show NRM intensities ranging between $1.65\cdot10^{-3}$ A/m and $16.4\cdot10^{-3}$ A/m, with a mean value of $7.59\cdot10^{-3}$ A/m, and magnetic susceptibility values between $177\cdot10^{-6}$ S.I and $380\cdot10^{-6}$ S.I. with a mean value of $256\cdot10^{-6}$ S.I. Results from the thermal demagnetization of the IRM applied to volcanic and volcaniclastic specimens from sites CC35, CC61, and CC63 (Fig. 3 A)

Table 2
Paleomagnetic data at site level of the High (Ch) and Low (Cl) temperature components in red beds. Sampled section and name of the site; coordinates (longitude and latitude); N: number of samples used to calculate the mean from the total number; Nt: number of total standard samples; Unit: stratigraphic unit, Transition Unit (TU), Lower Red Unit (LRU), Upper Red Unit (URU); site-mean NRM value; Km: site-mean susceptibility value, Declination (Dec) and Inclination (Inc) before (BTC) and after (ATC) tectonic correction; α_{95} and k are the statistical parameters of a fisherian distribution; Quality: good: $\alpha_{95} < 15$, intermediate: $\alpha_{95} = 15$ to 25, bad (out of threshold): $\alpha_{95} > 25$, D: declination error $D = \arcsin(\sin\alpha_{95} / \cos[I])$, S0: bedding plane (dip direction and dip).

	ETRS89 UTM zone31N EPSG: 25831			High temperature component (Ch)												
	Site	Longitude	Latitude	N	Nt	Unit	NRM .(A/m) ($\cdot 10^{-3}$)	Km ($\cdot 10^{-6}$)	Dec BTC	Inc BTC	α_{95}	Quality	D	k	Dec ATC	Inc ATC	S0 (D·D/Dip)
El Ges	CAD10 [x]	1.497620	42.28655	7	8	URU	4.96	176.6	350.8	12.4	14.4	good	15.1	18.63	354.6	17.8	104/15
	CAD11*	1.495580	42.28880	6	6	URU	1.65	181.6	178.9	42.5	38.5	bad	39.0	4.9	172.6	8.7	155/36
	CAD12*	1.490830	42.29010	8	8	URU	2.46	184.4	338.6	43.3	47.4	bad	–	2.32	288.0	70.6	185/39
	CAD13	1.499850	42.30048	5	8	LRU	6.64	247.6	144.8	54.1	8.4	good	8.8	83.28	170.8	17.8	202/48
				8★	8				159.3	68.5	17.8	intermediate	–	10.68	186.1	25.0	
Ansovell	CAD14	1.579020	42.30607	8	8	LRU	14.5	313.5	93.5	58.5	21.6	intermediate	30.8	7.53	158.6	44.0	202/48
Coll de Vanses	CAD15◦	1.547750	42.30281	8	8	LRU	6.18	229.3	5.1	41.2	12	good	43.4	31.55	352.8	72.4	193/32
	CAD17	1.540530	42.30491	6	8	LRU	16.4	380	117.0	60.6	10.6	good	12.5	28.03	149.1	31.6	180/40
	CAD18	2.033060	42.28189	7	7	LRU	6.05	337.7	174.3	35.3	10	good	11.0	37.18	173.9	−24.6	170/60
Castellar de n'Hug	CAD19	2.033557	42.28392	8	8	URU	13	–	166.9	45.2	5	good	5.0	123.92	177.2	−7.2	200/58
	CAD20	2.026621	42.28017	8	8	URU	4.1	–	75	40.4	3.2	good	3.3	303.39	120.3	15.5	172/74

				Low temperature component (Cl)												
	Site	Longitude	Latitude	N	Nt	Unit	NRM .(A/m) ($\cdot 10^{-3}$)	Km ($\cdot 10^{-6}$)	Dec BTC	Inc BTC	α_{95}	Quality	k	Dec ATC	Inc ATC	S0 (D·D/Dip)
El Ges	CAD10	1.497620	42.28655	7	8	URU	4.96	176.6	335.8	27	9.6	good	34.5	343.3	34.5	104/15
	CAD11*	1.495580	42.28880	6	6	URU	1.65	181.6	21.3	21.1	71.6	bad	2.63	40.3	42	155/36
	CAD12*	1.490830	42.29010	6	6	URU	2.46	184.4	6.2	28.6	28.3	bad	4.79	7.8	67.6	202/48
	CAD13*	1.499850	42.30048	5	8	LRU	6.64	247.6	32.3	16.1	71.5	bad	1.56	44	62.6	202/48
Ansovell	CAD14	1.579020	42.30607	8	8	LRU	14.5	313.5	359.8	29	12.9	good	22.76	320.7	67.9	202/48
Coll de Vanses	CAD15	1.547750	42.30281	8	8	LRU	6.18	229.3	331.7	24.0	23.6	intermediate	6.45	314.3	45.1	193/32
	CAD17	1.540530	42.30491	7	8	LRU	16.4	380	5.1	28.2	9.2	good	44.35	12.1	67.8	180/40
				8★	8				357.1	31.1	19.5	intermediate	9.01	352.3	71.0	
	CAD18*	2.033060	42.28189	7	–	LRU	–	–	–	–	–	–	–	–	–	–
Castellar de n'Hug	CAD19*	2.033557	42.28392	8	–	URU	–	–	–	–	–	–	–	–	–	–
	CAD20*	2.026621	42.28017	8	–	URU	–	–	–	–	–	–	–	–	–	–

* discarded sites: $\alpha_{95} > 25$ out of threshold or paleomagnetic component cannot be defined. ★ raw data. [x]transposed site (in the table mean direction without transposition, in stereoplot mean direction transposed). ◦ 5/8 specimens are remagnetized with the recent Earth's magnetic field

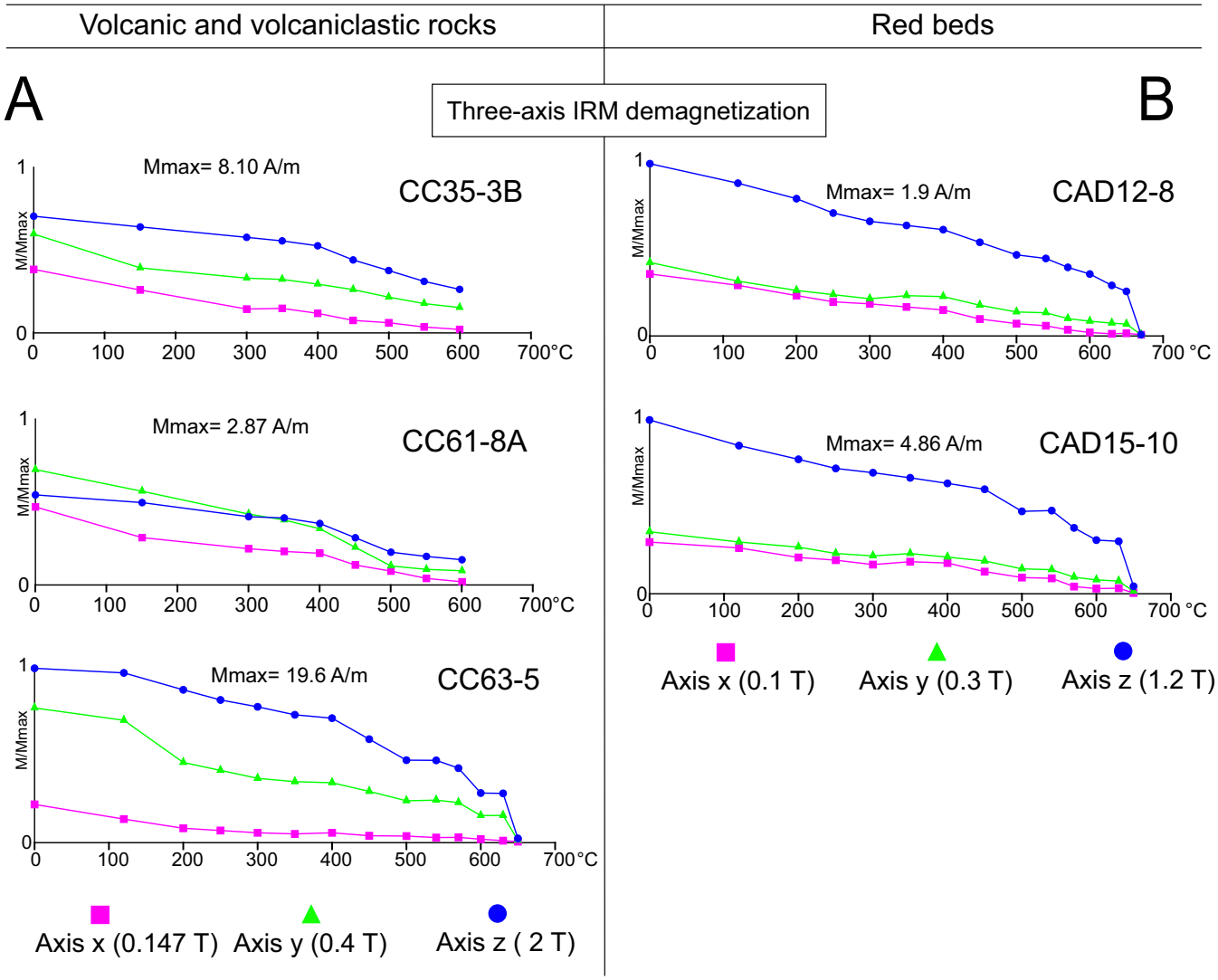

Fig. 3. A) Three-axis IRM thermal demagnetization in A) volcanic and volcaniclastic, and B) red beds specimens. (For interpretation of the references to colour in this figure legend, the reader is referred to the web version of this article.)

show that high coercivity minerals (2 T along the Z axis) such as hematite dominate in samples CC35 and CC63. Conversely, intermediate coercivity minerals (0.4 T, along the Y axis) are the main carriers for sample CC61. Sample CC63–5 showed a drop of magnetization at 200 °C, pointing toward the presence of an intermediate phase, probably goethite. The thermal demagnetization of the IRM applied to the red bed specimens (Fig. 3 B) from sites CAD12 and CAD15, shows that high coercivity minerals with high unblocking temperatures dominate (1.2 T along the Z axis). This is found in samples CC35, CC63, CAD12 and CAD15, and allows us to discard goethite and to consider hematite as the main carrier of the magnetization, instead. The presence of magnetite coexisting with the dominant hematite is also noticeable for both lithologies (site examples CC35, CC61, CAD12 and CAD15) where the soft coercivity component displays significant intensities that drop just below 600 °C.

Temperature-dependent susceptibility curves (Fig. 4, see also supplementary material) in volcanic and volcaniclastic rocks are irreversible. The heating curves present a concave hyperbolic shape at their beginning, indicating a paramagnetic contribution, a decay at 580 °C indicating the presence of magnetite (Tc 580 °C) and a final decay around 650–700 °C also indicating the presence of hematite. In the continental sedimentary rocks (red beds), susceptibility curves are almost reversible except for CAD10, CAD12, CAD14 and CAD18 where a magnetite phase is neoformed, as shown in the cooling curve. The heating curves show a small decay between 100 and 200 °C. This indicates the presence of a paramagnetic contribution, with an abrupt decay above 650 °C, and provides evidence for the presence of hematite. There are also slight, though noticeable decays below 600 °C, which point toward the presence of magnetite. In sample CAD13–1 the increase of susceptibility is associated with a broad Hopkinson's peak.

Diagrams of the normalized intensity of NRM versus temperature of the high temperature magnetic component (Fig. 5) in volcanic and volcaniclastic rocks show an abrupt decay at 580 °C for specimens CC40–1 and CC42b-6. For specimens CC36-4 A, and CC60-5 A, a slight decay at this temperature occurs before an abrupt decay close to 700 °C. In sedimentary rocks (red beds) the abrupt decay is above 610 °C, but a small decay is also noticeable around 580 °C for specimen CAD10–5.

4.2. *Demagnetization behavior and paleomagnetic components*

We separated the sampling sites into two groups depending on their lithological type. The identified components span the following temperature intervals:

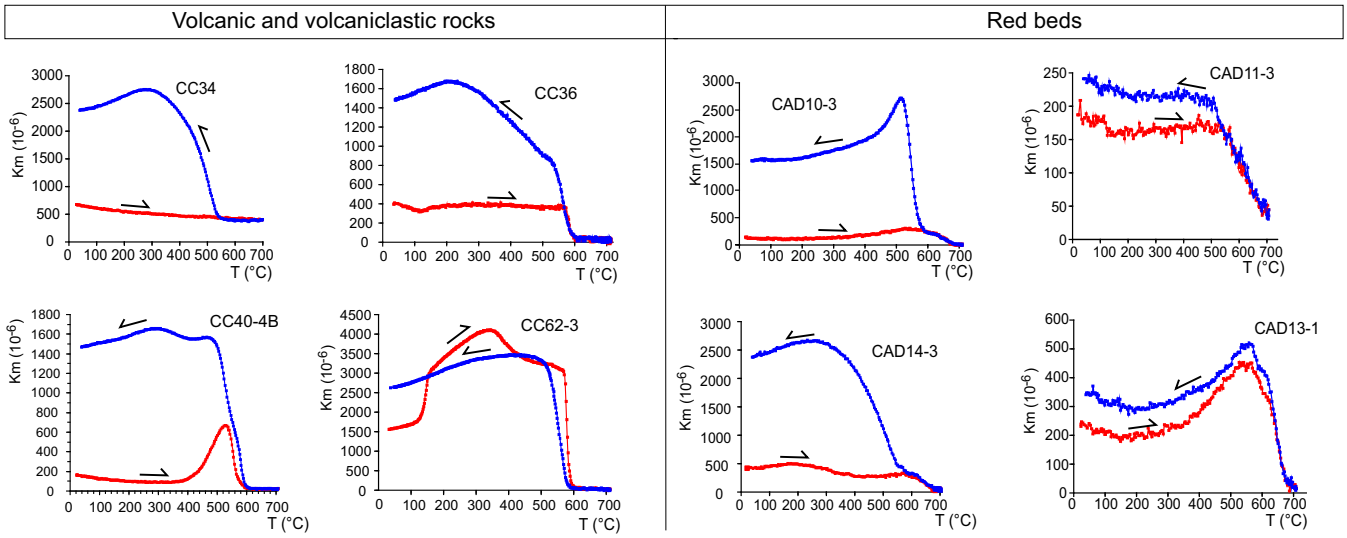

Fig. 4. Representative susceptibility-temperature curves in volcanic and volcaniclastic rocks and red beds. Heating curve in red and cooling curve in blue. See curves for all specimens in the Supplementary material. (For interpretation of the references to colour in this figure legend, the reader is referred to the web version of this article.)

- *Volcanic-volcaniclastic rocks*: the low temperature component presents a maximum unblocking temperature of 300 °C (Fig. 5). The high temperature paleomagnetic component presents an unblocking temperature from 480 °C, although it occasionally starts at 350 °C. This component is defined up to a maximum value that normally reaches 570–600 °C, although in some specimens it extends to 650–670 °C.
- *Sedimentary red beds:* the low temperature paleomagnetic component is defined between 100 and 200 °C and 300–350 °C, although in some specimens it reaches up to 400–450 °C. The high temperature paleomagnetic component for the red beds presents an unblocking temperature between a minimum value in the range of 350–450 °C and a maximum value that extends up to 650 °C (Fig. 5). This interval is similar to the one defined for the volcaniclastic rocks.

Diagrams of the normalized intensity of NRM versus temperature show a complete decay at 630 to 670 °C, both in the volcanic rocks and in the sedimentary red beds, although for some specimens of volcanic rocks this decay occurs at 570 to 580 °C (Fig. 5).

According to these temperature intervals, the high temperature characteristic paleomagnetic components obtained for the different analyzed transects are as follows (Fig. 5):

- *Argestués outcrop* (sites CC70 and CC75, volcaniclastic rocks): the paleomagnetic directions during stepwise thermal demagnetization are randomly distributed for all the specimens and paleomagnetic components cannot be isolated (Fig. 2 B).
- *El Ges transect* (sites CC34, CC36, CC37 and CC40 for the volcanic sequence and CAD10, CAD11, CAD12, CAD13 for the red beds). For the volcaniclastic rocks, the paleomagnetic signal in each specimen is good and gives well-defined directions, except for sites CC34, CC36 and CC37. The mean values at site level (Table 1) display a high degree of scattering ($\alpha_{95} > 50°$) and the obtained paleomagnetic component was discarded. Site CC40 shows a good clustering ($\alpha_{95} = 7.5°$). In the red beds, the paleomagnetic signal for each specimen is good to intermediate and gives well-defined directions, except for sites CAD11 and CAD12. The mean values at site level display a remarkable degree of scattering ($\alpha 95 > 30°$) and were also discarded. For sites CAD10 and CAD13, the mean values for the sampling sites show good quality (α_{95} of 14.4° and 8.4°, respectively) (Table 2).
- *Coll de Vanses transect* (sites CC60, CC61, CC62, CC63, CC65, CC66, CC67 and CC68 in the volcanic sequence and CAD15 and CAD17 in the red beds). For the volcaniclastic sites, the individual paleomagnetic directions at site level and the site average are of good quality and are well-clustered (α_{95} between 3.1° and 16.3°). The red beds sites present a good paleomagnetic signal and their degree of dispersion is similar to the one observed in El Ges ($\alpha_{95} = 12°$ and 10.6°, respectively). Nevertheless, the mean direction at site CAD15 suggests a recent remagnetization under the (normal) present-day Earth's magnetic field and has been excluded from further consideration (Table 2).
- *Ansovell transect* (sites CC42, CC54 and CC55 in volcaniclastic materials and CAD14 in red beds). These sites show a good paleomagnetic signal quality for each specimen and good grouping at the site level, both for the volcaniclastic sequence (α_{95} between 1.5° and 3.4°). and for the red beds ($\alpha_{95} = 21.6°$ for site CAD14). Site CC54 displays a paleomagnetic direction that has not been observed in any of the other studied sites or in previous studies carried out in the area (Fig. 6).
- *-Castellar de n'Hug outcrop* (CAD18, CAD19 and CAD20 sites, in red beds). These sites show a well-defined paleomagnetic component with clusterings that show α_{95} values from 3.2° to 10°.

A low temperature paleomagnetic component was recognized 1) in the volcanic and volcaniclastic rocks except at sites CC61 and CC63, and 2) in the red beds (Fig. 7), except for those located in the Castellar de n'Hug zone. Sites CAD10, CAD14, CAD15 and CAD17 are the only sites considered (α_{95} between 9.6° and 23.6°, Fig. 7).

Only two sites (CC62 and CAD17) present anomalous directions that were therefore excluded from the group statistics and the mean paleomagnetic component calculation. These individual specimens were rejected because they present a random orientation with respect to the rest of the specimens of the site, which, conversely, were clearly grouped (in Tables 1 and 2 we show the effect of rejection of anomalous data on the mean direction and associated confidence cone). At three sampling sites no component could be defined for any of the specimens (CC35, CC70 and CC75).

5. Interpretation and Discussion

5.1. Paleomagnetic directions and age of magnetization

The low-temperature component in volcanic and volcaniclastic rocks is probably a viscous component and corresponds to the recent or

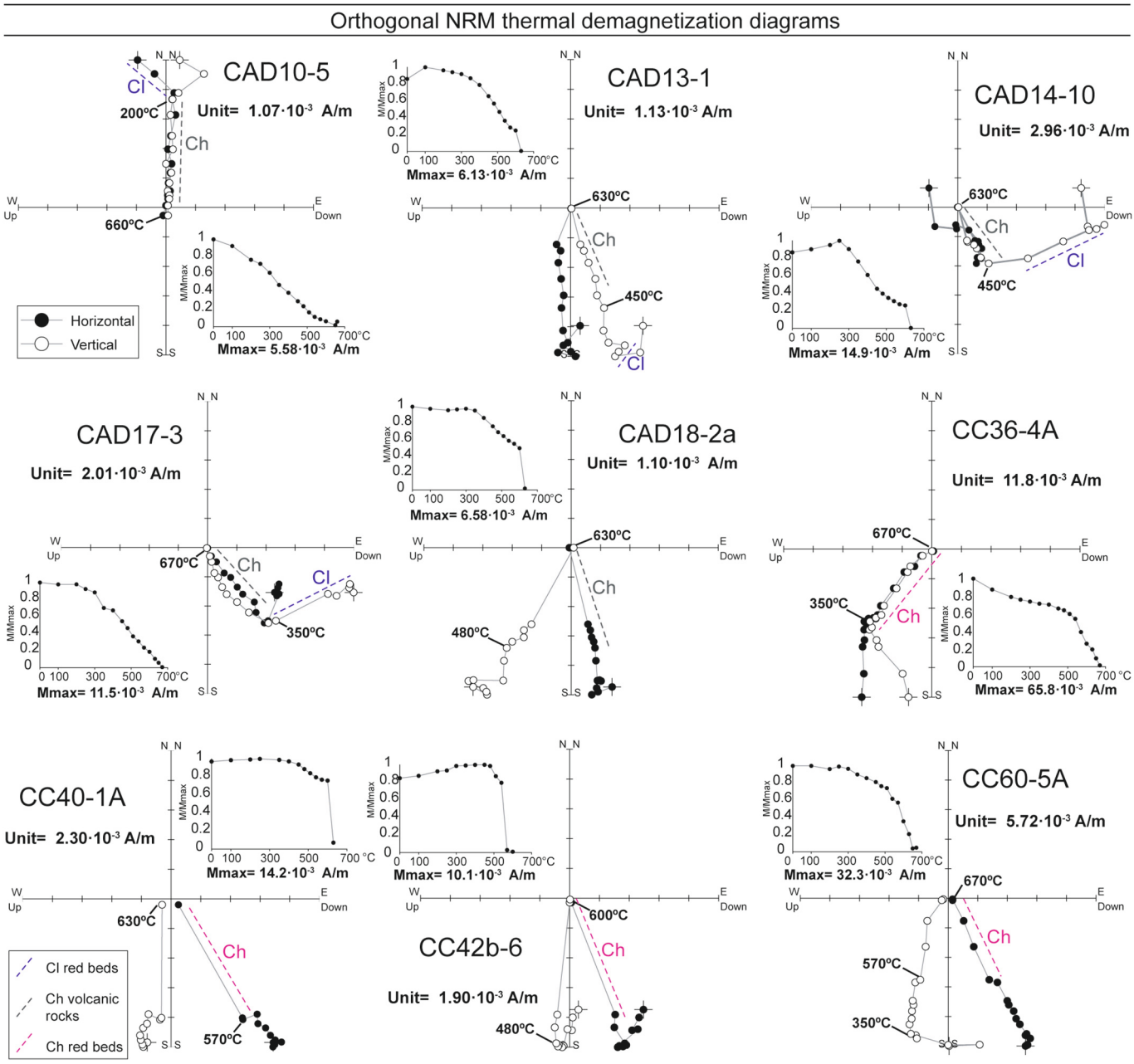

Fig. 5. Orthogonal NRM thermal demagnetization diagrams of representative specimens from the Carboniferous volcanic and volcaniclastic rocks (CC36-4a, CC40–1 A, CC42b-6 and CC60-5 A) and Permian red beds (CAD10–5, CAD13–1, CAD14–10, CAD17–3 and CAD18-2 A). Vertical projection in white and horizontal projection in black; N upward and E to the right. Normalized intensity of the NRM (M/Mmax) versus temperature diagrams are also shown. (For interpretation of the references to colour in this figure legend, the reader is referred to the web version of this article.)

current magnetic field direction for in situ coordinates. The low-temperature component in the red beds appears well-grouped and shows normal polarity. It does not reach the expected recent magnetic field orientation, either in situ or after total restoration, but the path from one direction to the other parallels the paleomagnetic reference for the Eocene-Oligocene interval (Fig. 7). Because of that, we interpreted this low-temperature component as a *syn*-tectonic secondary direction probably acquired during the Cenozoic (Early Eocene-Oligocene). It was during that period (50 to 20 Ma approximately), that the Pyrenean compression showed its maximum intensity (Vergés et al., 2002). This low-temperature paleomagnetic component was only detected in the central zone of the Cadí Basin (sites CAD10, CAD11, CAD12, CAD13, CAD14, CAD15 and CAD17) and not in its easternmost part (Castellar de n'Hug area, sites CAD18, CAD19 and CAD20).

The high temperature paleomagnetic component was isolated both in the volcanic-volcaniclastic rocks of Carboniferous age and in the Permian red beds (Fig. 8).

For the volcanic-volcaniclastic rocks, sites CC34, CC36 and CC37 present an important internal degree of scattering and site CC54 displays an anomalous paleomagnetic direction that has not been observed at any of the other studied sites or in previous studies carried out in the area, hence they were not further considered (Table 1).

Considering all the directions at the site level (Fig. 9), the resulting mean paleomagnetic direction has a declination of 154.8° and an inclination of −0.3° after bedding correction ($N = 11$, $R = 10.44$, $k = 17.78$ and $\alpha_{95} = 11.1°$) in the volcanic and volcaniclastic rocks. In the continental sedimentary rocks (red beds), the resulting mean paleomagnetic direction shows a declination of 160.8° and an inclination of

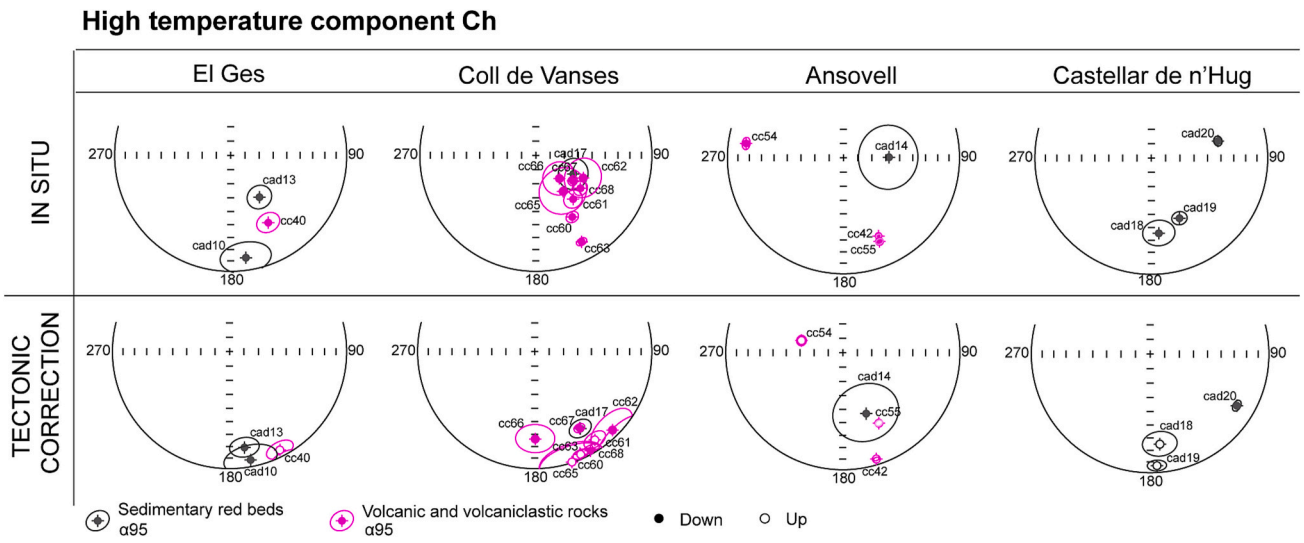

Fig. 6. High temperature paleomagnetic component and α_{95} confidence cone for each site in both lithologies (volcanic rocks and red beds) in the studied zones of the Cadí Basin, in situ and after tectonic correction. (For interpretation of the references to colour in this figure legend, the reader is referred to the web version of this article.)

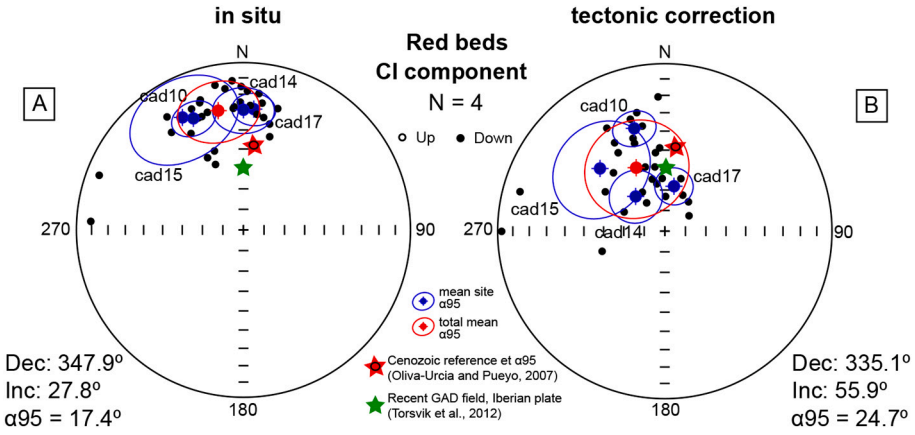

Fig. 7. Paleomagnetic results of the low temperature component at site level: A) in situ (Dec. = 347.9, Inc. = 27.8) and B) after tectonic correction (Dec. = 355.1, Inc. = 55.9). The Cenozoic reference (Late Eocene-Early Oligocene) calculated from sediments of stable Iberia is Dec. = 005, Inc. = 47, α_{95} = 2, k = 16 (Oliva-Urcia and Pueyo, 2007).

13.6° after the bedding correction ($N = 7$, $R = 6.12$, k = 6.78 and α_{95} = 23.6°).

The high temperature components isolated in the volcanic-volcaniclastic rocks (Carboniferous-Permian age) and the red beds (Permian age) are similar both in declination and inclination, and are indistinguishable from a statistical point of view. Individual sites show a dominant reverse polarity, and very low inclinations (Figs. 8 and 9). After tectonic correction, the resulting paleomagnetic directions in the two sampled lithologies coincide with the Permian reference direction for the Pyrenees (D = 166, I = -9, Oliva-Urcia et al., 2012) (Fig. 9). The main magnetic carriers of the magnetization in both lithologies are magnetite and hematite as observed in the results of the 3-axis IRM and the susceptibility-temperature curves. In the first experiment, the presence of a high coercivity mineral, which points toward the presence of hematite in both lithologies, is clearly visible. In the susceptibility-temperature curves the decay for hematite is not visible, probably because magnetite has an intrinsic susceptibility of at least 10^3–10^4 times higher than hematite, while the multiplying factor for saturation remanence is only 50.

In any case, the dominant reverse component shows a very low inclination after tectonic correction which is compatible with the primary reverse polarity magnetization retrieved for the Permian red beds. The high-temperature component of the volcanic rocks could also be primary in origin, but the similarity of the orientation of the paleomagnetic vectors in relation to the red beds, in spite of their older age, points to a secondary origin of this magnetization. If the remagnetization is chemical in origin, as may be suggested by the strong, early alteration of minerals in the volcanic series (Bixel, 1984), it should have occurred before the deposition of the overlying red beds. The chemical origin for this (probable) remagnetization is also reinforced by the non-reversibility of the susceptibility-temperature curves. This non-reversibility indicates that these minerals are not thermally stable and did not undergo high temperatures since their formation. Alternatively, fluid circulation at the end of the rifting stage could have involved only the lower part of the sequence (i.e., volcanic and volcaniclastic rocks), whose permeability was enhanced by pervasive fracturing related to extensional tectonics. Conversely, the clayey levels within the red bed units could have worked as a thermal and chemical seal for the ascent of magnetite- and hematite-bearing fluids (see, e.g. Johnson et al., 1995; Eichhubl et al., 2009; Nemkin et al., 2016; Skurtveit et al., 2018; Zhang et al., 2020).

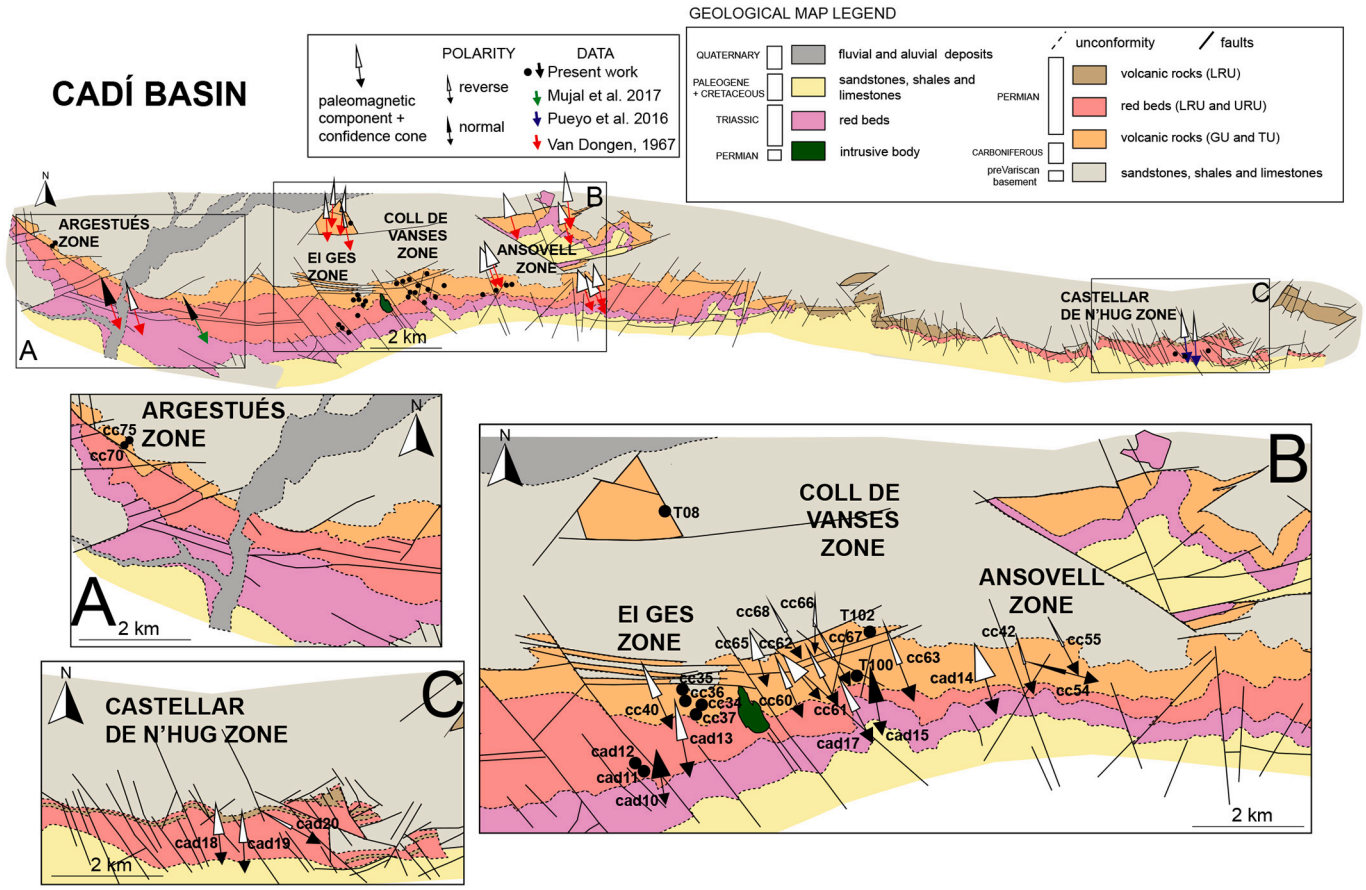

Fig. 8. A) Map view of the Cadí Basin (Modified from Gisbert, 1981) with the previous paleomagnetic data and the high temperature components. The α_{95} confidence cone isolated in the present study in the studied zones is also shown. A) Argestués area, B) El Ges, Coll de Vanses and Ansovell areas, and C) Castellar de n'Hug areas; all diagrams after tectonic correction. See Tables 1 and 2 for the declination error. D. Sites T08, T100 and T102 are the discarded conglomerate tests.

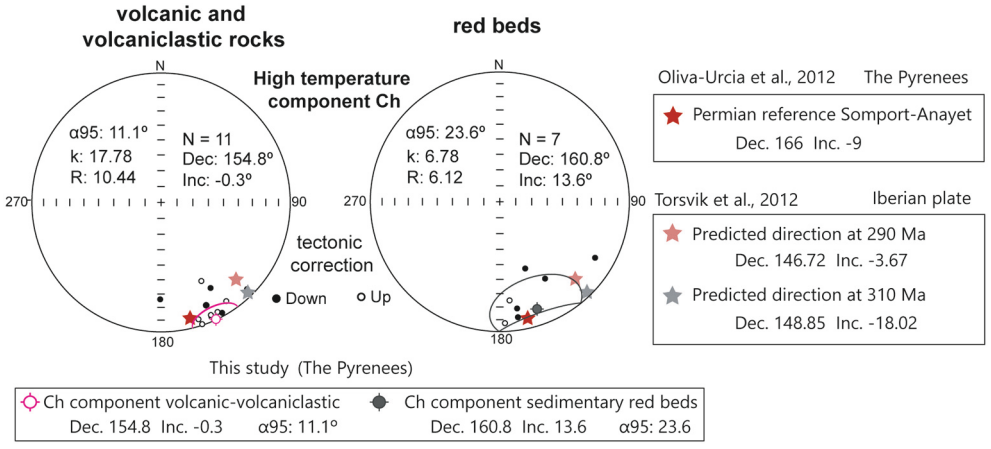

Fig. 9. Stereoplots showing the Permian reference in the Pyrenees (Oliva-Urcia et al., 2012), the predicted Permian and Carboniferous directions (after Koymans et al., 2016) using paleomagnetic directions from Iberia (Torsvik et al., 2012) and the high temperature paleomagnetic component in volcanic-volcaniclastic rocks and red beds from this study. (For interpretation of the references to colour in this figure legend, the reader is referred to the web version of this article.)

5.2. *Implications for the kinematics of basement thrust sheets*

The Pyrenees represent one of the areas in the world with a higher number of paleomagnetic studies both for tectonic and magnetostratigraphic objectives (San Miguel et al., 2010). In spite of that, the Late Carboniferous-Permian Cadí Basin, located in the Eastern Pyrenees, has been the focus of very few previous works, some of which showing contradictory results. The paleomagnetic directions in the Permian volcanic rocks (Van Dongen, 1967) were related to an Early Permian primary magnetization that shows a deviation attributed to a post-Permian counterclockwise rotation of the Iberian plate. In the Permian red beds, Pueyo et al. (2016b) isolated a primary magnetization showing a direction similar to the results obtained by Van Dongen (1967). Those authors also isolated an intermediate-temperature reverse paleomagnetic component for these sites. Conversely, a generalized remagnetization in the Permian red beds was proposed by Mujal et al. (2017).

Close to the study area, Gil-Peña et al. (2006) sampled Ordovician rocks below the Stephanian unconformity and obtained a secondary paleomagnetic magnetization, probably related to a remagnetization event linked to the formation of the Late Carboniferous-Permian Cadí Basin. These results fit better with the early remagnetization hypothesis vs. primary magnetization in the volcaniclastic rocks, as indicated in the previous point, although it cannot be considered as definitive, either.

Paleomagnetic studies have also been done in equivalent volcaniclastic rocks that belong to a contemporaneous basin located to the west, the Late Carboniferous-Permian Castejón-Las Paules Basin (Izquierdo-Llavall et al., 2013, 2018). These authors found a primary paleomagnetic magnetization both in the volcanic rocks and in the overlying Triassic red beds. Vertical axis rotations in that basin are linked to the upper Alpine thrust units (downward facing structures included in the Nogueres Zone; e.g., Séguret, 1972; Saura and Teixell, 2006), whereas the lower ones (equivalent to the Orri thrust unit) are not rotated.

In our study, the coincidence of the paleomagnetic directions with the Permian reference indicates the absence of vertical axis rotations for the Cadí Basin, and hence for the Orri basement thrust sheet. This confirms a strong lateral continuity of basement-involved Pyrenean thrust units. In fact, the Castejón-Las Paules Basin was incorporated during the Alpine orogeny in the antiformal stack of the Axial Zone in the same way as the Cadí Basin. Moreover, the absence of significant vertical-axis rotations in the Orri thrust sheet is also supported by the paleomagnetic directions of a low temperature component that postdates structures associated with the Pyrenean compression (Eocene-Oligocene). In the same sense, the fact that the high temperature component direction (Ch) after bedding correction is close to the expected Permian reference, indicates a pre-folding acquisition of the remagnetization (before the Alpine period and the tilting of the whole stratigraphic succession).

6. Conclusions

The paleomagnetic analysis of volcanic, volcanoclastic rocks and red beds of Late Carboniferous and Permian ages from the Eastern Pyrenees allows us to conclude the following:

- There are not significant differences between the high temperature paleomagnetic directions obtained in the red beds and the ones obtained in volcanic and volcaniclastic rocks. This suggests either a primary acquisition with little or no change throughout time, or a remagnetization for the volcanic series co-existing with (i) a primary magnetization for the red beds or, alternatively (ii) an early Permian remagnetization just after their deposition, always consistent with the poles for the Iberian plate at this stage.
- The high temperature component direction is close to the expected Permian reference after bedding correction and therefore it predates the folding of beds. This implies a Cenozoic compressional origin for folding, which excludes tilting associated with previous rifting processes.
- The coincidence of the obtained paleomagnetic directions with the Permian reference indicates the absence of vertical axis rotations for the Cadí Basin, and hence for the Orri basement thrust sheet.

Supplementary data to this article can be found online at https://doi.org/10.1016/j.tecto.2023.230148.

CRediT authorship contribution statement

Ana Simón-Muzás: Writing – review & editing, Writing – original draft, Visualization, Resources, Methodology, Investigation, Data curation. **Antonio M. Casas-Sainz:** Writing – review & editing, Supervision, Project administration, Investigation, Funding acquisition, Conceptualization. **Ruth Soto:** Writing – review & editing, Supervision, Project administration, Investigation, Funding acquisition, Conceptualization. **Emilio L. Pueyo:** Supervision, Resources, Methodology, Investigation. **Elisabet Beamud:** Supervision, Resources, Methodology, Investigation. **Belén Oliva-Urcia:** Supervision, Resources, Investigation.

Declaration of Competing Interest

The authors declare that they have no known competing financial interests or personal relationships that could have appeared to influence the work reported in this paper.

Data availability

Data in the article and in supplementary material. The .rs3 data will be sent upon request.

Acknowledgements

This work was supported by projects grants PID2020-114273GB-C22, PID2019-108753GB-C22, and PID2019-104693GB-I00 funded by MCIN/AEI/10.13039/501100011033, "ERDF Away of making Europe" and grant FPU19/02353 funded by MCIN/AEI/10.13039/501100011033, "ERDF Away of making Europe" and funded by "ESF Investing in your future". This study represents a contribution from the GeoAp (E01-20R) and the GeoTransfer (E32-20R) Research Groups (Aragón Government). EB thanks the Geomodels Research Institute and AGAUR 2021SGR00076. Thanks are given to Gaia Siravo, Juan José Villalaín, P. Robion and the editor Gideon Rosenbaum for their detailed review of the manuscript and their suggestions.

References

Barnolas, A., Pujalte, V., 2004. La Cordillera Pirenaica. Geol. Espan. 233–241.
Bixel, F., 1984. Le volcanisme Stephano-Permien des Pyrenees (These du Grade de Docteur d'Etat). Université Paul Sabatier du Tolouse.
Casas, J.M., Queralt, P., Mencos, J., Gratacós, O., 2012. Distribution of linear mesostructures in oblique folded surfaces: Unravelling superposed Ordovician and Variscan folds in the Pyrenees. J. Struct. Geol. 44, 141–150.
Chadima, M., Hrouda, F., 2006. Remasoft 3.0 – a user-friendly paleomagnetic data browser and analyzer. Travaux Géophys. XXVII, 1980, 20–21 Coward,M.P.
Chadima, M., Hrouda, F., 2012. Cureval 8.0: Thermomagnetic Curve Browser for Windows. Agico, Inc.
Eichhubl, P., Davatz, N.C., Becker, S.P., 2009. Structural and diagenetic control of fluid migration and cementation along the Moab fault, Utah. AAPG Bull. 93 (5), 653–681.
Fisher, R.A., 1953. Dispersion on a sphere. Proc. Roy. Soc. Lond. Ser. A. Math. Phys. Sci. 217 (1130), 295–305.
Garcés, M., García-Senz, J., Muñoz, J.A., López-Mir, B., Beamud, E., 2016. Timing of magnetization and vertical-axis rotations of the Cotiella massif (late cretaceous, South Central Pyrenees). Geol. Soc. Lond. Spec. Publ. 425 (1), 213–232.
Gil-Peña, B., Oliva, E.L., Pueyo, A. Barnolas, 2006. Datos preliminares de la remagnetización Estephaniense del Ordovícico Superior del Pirineo Centro-meridional; implicaciones estructurales. MagIber IV-Vigo, 47–50.
Gisbert, J., 1981. Estudio Geológico - Petrológico del Estefaniense – Pérmico de la Sierra del Cadi (Pirineo de Lérida). Diagenesis y Sedimentología. Unpublished Ph DUniversidad de Zaragoza, p. 472.
Gong, Z., Langereis, C.G., Mullender, T.A.T., 2008. The rotation of Iberia during the Aptian and the opening of the Bay of Biscay. Earth Planet. Sci. Lett. 273 (1–2), 80–93.
Izquierdo-Lavall, E., Casas-Sainz, A.M., Oliva-Urcia, B., Burtmester, R., Pueyo, E.L., Housen, B., 2015. Multi-episodic remagnetization related to diachronous thrusting in the Pyrenean Internal Sierras. Geophys. J. Int. 201, 891–914.
Izquierdo-Llavall, E., Casas-Sainz, A., Oliva-Urcia, B., Scholger, R., 2013. Palaeomagnetism and magnetic fabrics of the late Palaeozoic volcanism in the Castejón-Laspaúles basin (Central Pyrenees). Implications for palaeoflow directions and basin configuration. Geol. Mag. 151 (5), 777–797.
Izquierdo-Llavall, E., Casas-Sainz, A.M., Oliva-Urcia, B., Villalaín, J.J., Pueyo, E.L., Scholger, R., 2018. Rotational kinematics of basement antiformal stacks: paleomagnetic study of the western Nogueras Zone (Central Pyrenees). Tectonics 37 (10), 3456–3478.
Johnson, S.A., Turner, P., Hartley, A., Rey, D., 1995. Palaeomagnetic implications for the timing of hematite precipitation and remagnetization in the Carboniferous Barren Red measures, UK southern North Sea. Geol. Soc. Lond. Spec. Publ. 98 (1), 97–117.
Koymans, M.R., Langereis, C.G., Pastor-Galan, D., van Hinsbergen, D.J.J., 2016. Paleomagnetism.org: an online multi-platform open source environment for paleomagnetic data analysis. Comput. Geosci. 93, 127–137.
Larrasoaña, J.C., Parés, J.M., del Valle, J., Millán, H., 2003. Triassic paleomagnetism from the Western Pyrenees revisited: implications for the Iberian–Eurasian Mesozoic plate boundary. Tectonophysics 362 (1–4), 161–182.

Lowrie, W., 1990. Identification of ferromagnetic minerals in a rock by coercivity and unblocking temperature properties. Geophys. Res. Lett. 17 (2), 159–162.
McCaig, A.M., McClelland, E., 1992. Palaeomagnetic techniques applied to thrust belts. Thrust Tecton. 209–216.
Mujal, E., Fortuny, J., Pérez-Cano, J., Dinarès-Turell, J., Ibáñez-Insa, J., Oms, O., Anadón, P., 2017. Integrated multi-stratigraphic study of the Coll de Terrers late Permian–Early Triassic continental succession from the Catalan Pyrenees (NE Iberian Peninsula): a geologic reference record for equatorial Pangaea. Glob. Planet. Chang. 159, 46–60.
Muñoz, J.A., 1992. Evolution of a continental collision belt: ECORS-Pyrenees crustal balanced cross-section. In: Thrust Tectonics. Springer, Dordrecht, pp. 235–246.
Muñoz, J.A., Martínez, A., Vergés, J., 1986. Thrust sequences in the eastern Spanish Pyrenees. J. Struct. Geol. 8 (3–4), 399–405.
Nemkin, S.R., Lageson, D., van der Pluijm, B., Van der Voo, R., 2016. Remagnetization and folding in the frontal Montana Rocky Mountains. Lithosphere 8 (6), 716–728.
Oliva-Urcia, B., Pueyo, E.L., 2007. Rotational basement kinematics deduced from remagnetized cover rocks (Internal Sierras, southwestern Pyrenees). Tectonics 26 (4).
Oliva-Urcia, B., Pueyo, E.L., 2019. Paleomagnetism in structural geology and tectonics (review chapter). In: Mukherjee S (Ed) Teaching Methodologies in Structural Geology and Tectonics. Soumyajit Mukherjee Springer, Heidelberg, pp. 55–121 (ISBN: 978-981-13-2781-0).
Oliva-Urcia, B., Pueyo, E.L., Larrasoaña, J.C., 2008. Magnetic reorientation induced by pressure solution: a potential mechanism for orogenic-scale remagnetizations. Earth Planet. Sci. Lett. 265 (3–4), 525–534.
Oliva-Urcia, B., Pueyo, E.L., Larrasoaña, J.C., Casas, A.M., Román-Berdiel, T., Van der Voo, R., Scholger, R., 2012. New and revisited paleomagnetic data from Permian–Triassic red beds: two kinematic domains in the west-central Pyrenees. Tectonophysics 522, 158–175.
Pastor-Galán, D., Groenhof, O., Pueyo, E.L., Izquierdo-Llaval, E., Dinarès-Turell, J., Dekkers, M.J., 2021. Paleomagnetism from multiorogenic terranes is "not a simple game": Pyrenees' Paleozoic warning. Geophys. J. Int. 227 (2), 849–874.
Pereira, M.F., Castro, A., Chichorro, M., Fernández, C., Díaz-Alvarado, J., Martí, J., Rodríguez, C., 2014. Chronological link between deep-seated processes in magma chambers and eruptions: Permo-Carboniferous magmatism in the core of Pangaea (Southern Pyrenees). Gondwana Res. 25, 290–308.
Pueyo, E.L., Oliva-Urcia, B., Sussman, A.J., Cifelli, F., 2016a. In: Pueyo, E.L., Cifelli, F., Sussman, A., Oliva-Urcia, B. (Eds.), Palaeomagnetism in Fold and Thrust Belts: Use with caution. Geological Society of London Special Publication on Palaeomagnetism in Fold and Thrust Belts: New Perspectives, vol. 425 (1), pp. 259–276.
Pueyo, E.L., Beamud, E., Muñoz, J.A., Rodríguez-Pintó, A., San Miguel, G., 2016b. Remagnetización alpina en la Serra del Cadí (Pirineo Oriental). Geotemas 16 (1), 869–872.
Ramón, M.J., Pueyo, E.L., Oliva-Urcia, B., Larrasoaña, J.C., 2017. Virtual directions in paleomagnetism: a global and rapid approach to evaluate the NRM components. Front. Earth Sci. 5, 8.
San Miguel, G., Hernández, R., Pueyo, E.L., 2010. Pyrenean Paleomagnetic Database; Concept, state-of-the-art, and web interface design. Resúm. MAGIBER VI-Paleomagnet. Espan. Portug. 50–53.
Saura, E., Teixell, A., 2006. Inversion of small basins: effects on structural variations at the leading edge of the Axial Zone antiformal stack (Southern Pyrenees, Spain). J. Struct. Geol. 28 (11), 1909–1920.
Séguret, M., 1972. Étude tectonique des nappes et séries décollées de la partie centrale du versant sud des Pyrénées. Pub. Estela. Ser Geol. Struct. 2, 1–155.
Simón-Muzás, A., Casas-Sainz, A.M., Soto, R., Gisbert, J., Román-Berdiel, T., Oliva-Urcia, B., Pueyo, E.L., Beamud, E., 2022. Axial longitudinal flow in volcanic materials of the late Carboniferous-Permian Cadí basin (Southern Pyrenees) determined from anisotropy of magnetic susceptibility. J. Volcanol. Geotherm. Res. 421, 107443.
Skurtveit, E., Miri, R., Hellevang, H., 2018. Fluid-Rock Interactions in Clay-Rich Seals: Impact on Transport and Mechanical Properties. Geological Carbon Storage: Subsurface Seals and Caprock Integrity, pp. 167–185.
Soto, R., Villalaín, J.J., Casas-Sainz, A.M., 2008. Remagnetizations as a tool to analyze the tectonic history of inverted sedimentary basins: a case study from the Basque-Cantabrian basin (North Spain). Tectonics 27 (1).
Soto, R., Casas-Sainz, A.M., Villalaín, J.J., 2011. Widespread cretaceous inversion event in northern Spain: evidence from subsurface and palaeomagnetic data. J. Geol. Soc. Lond. 168 (4), 899–912.
Soto, R., Clariana, P., Ayala, C., Rey-Moral, C., Casas-Sainz, A.M., Román-Berdiel, T., Margalef, A., Rubio, F., Oliva-Urcia, B., Pueyo, E.L., Martín-León, J., Beamud, E., 2022. Assessing the internal uppermost crustal structure of the central pyrenees by gravity-constrained cross sections. Tectonics 41 (8) e2021TC007009.
Sussman, A.J., Pueyo, E.L., Chase, C.G., Mitra, G., Weil, A.B., 2012. The impact of vertical-axis rotations on shortening estimates. Lithosphere 4 (5), 383–394.
Torres-López, S., Casas, A.M., Villalaín, J.J., Moussaid, B., Ruiz Martínez, V.C., El-Ouardi, H., 2018. Evolution of the ridges of Midelt-Errachidia section in the high atlas revealed by paleomagnetic data. Tectonics 37 (9), 3018–3040.
Torsvik, et al., 2012. Phanerozoic polar wander, palaeogeography and dynamics source of the Document. Earth Sci. Rev. 114 (3–4), 325–368.
Van Dongen, P.G., 1967. The rotation of Spain: palaeomagnetic evidence from the eastern Pyrenees. Palaeogeogr. Palaeoclimatol. Palaeoecol. 3, 417–432.
Vergés, J., Fernàndez, M., Martínez, A., 2002. The Pyrenean orogen: pre-, syn-, and post-collisional evolution. In: Rosenbaum, G. and Lister, G. S. 2002. Reconstruction of the evolution of the Alpine-Himalayan Orogen. J. Virtual Explor. 8, 55–74.
Villalaín, J.J., Casas-Sainz, A.M., Soto, R., 2016. Reconstruction of inverted sedimentary basins from syn-tectonic remagnetizations. A methodological proposal. Geol. Soc. Lond. Spec. Publ. 425 (1), 233–246.
Vissers, R.L.M., Meijer, P.T., 2012. Mesozoic rotation of Iberia: Subduction in the Pyrenees? Earth Sci. Rev. 110 (1–4), 93–110.
Zhang, Y., Jia, D., Muxworthy, A.R., Zhang, Y., Li, Y., Yin, H., Chen, Z., Brzozowski, M., Li, W., Wang, M., Li, Z., 2020. Fluid migration and widespread remagnetization in the Dabashan fold and thrust belt, China. J. Geophys. Res. Solid Earth 125 (11) e2020JB019989.
Zijderveld, J.D.A., 1967. A.C. Demagnetization of rocks: Analysis of results. In: Collinson, D.W., Creen, K.M., Runcorn, S.K. (Eds.), Methods in Paleomagnetism. Elsevier, Amsterdam.